Supplementary information

Elucidating the stabilizing effect of copper substitution in high voltage P2–type layered oxides for sodium ion batteries

Remy Lecordier[1,2], Jon Serrano–Sevillano[1*], Amaia Saracibar[3], Carlos Escudero[4], Gaël Minart[1], Naiara Etxebarria[1], François Fauth[4], Carlo Marini[4], Alessandro Longo[5,6], Lorenzo Stievano[7,8,9], Marcus Fehse[1,9], Damien Saurel[1*]

[1] Center for Cooperative Research on Alternative Energies (CIC energiGUNE), Basque Research and Technology Alliance (BRTA), Parque Tecnológico de Álava, Albert Einstein 48, 01510 Vitoria–Gasteiz, Spain

[2] Materials Science and Technology Department, Basque Country University, Bilbao, Bizkaia, Spain

[3] Physical Chemistry Department, Pharmacy Faculty, Basque Country University, Vitoria–Gasteiz, Álava, Spain

[4] CELLS–ALBA Synchrotron Light Source, Cerdanyola del Vallès 08290, Spain

[5] BM16–FAME Beamline The European Synchrotron Research Facility 71 Avenue des Martyrs, F–38000, Grenoble, France

[6] Istituto Studio dei Materiali Nanostrutturati–CNR, Consiglio Nazionale delle Ricerche, 90146 Palermo, Italy

[7] Institut Charles Gerhardt Montpellier (ICGM), Univ. Montpellier, CNRS, 34293 Montpellier, France

[8] Réseau sur le Stockage Electrochimique de l'Energie (RS2E), CNRS, 80039 Amiens, France

[9] ALISTORE–ERI European Research Institute, CNRS, 80039 Amiens, France

[*]e–mail: dsaurel@cicenergigune.com; jserrano@cicenergigune.com

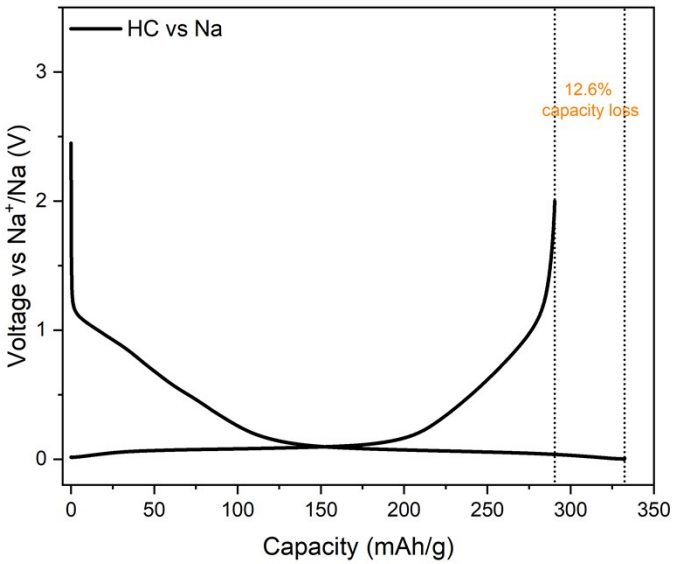

Figure S1. *First electrochemical cycle of the hard carbon anode vs. Na^+/Na in half–cell configuration. Galvanostatic charge–discharge curves were collected at a current density of C/15 (1C = 372 mA g^{-1}) between 0.005–2.0 V.*

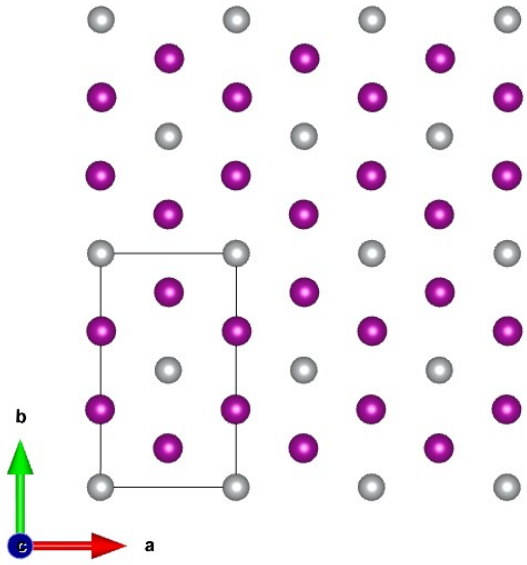

Figure S2. *Top view of the transition metal layer used in DFT calculations, showing the fixed, ordered honeycomb–like arrangement of Mn (purple) and Ni or Cu (grey) atoms within the P2–type structure.*

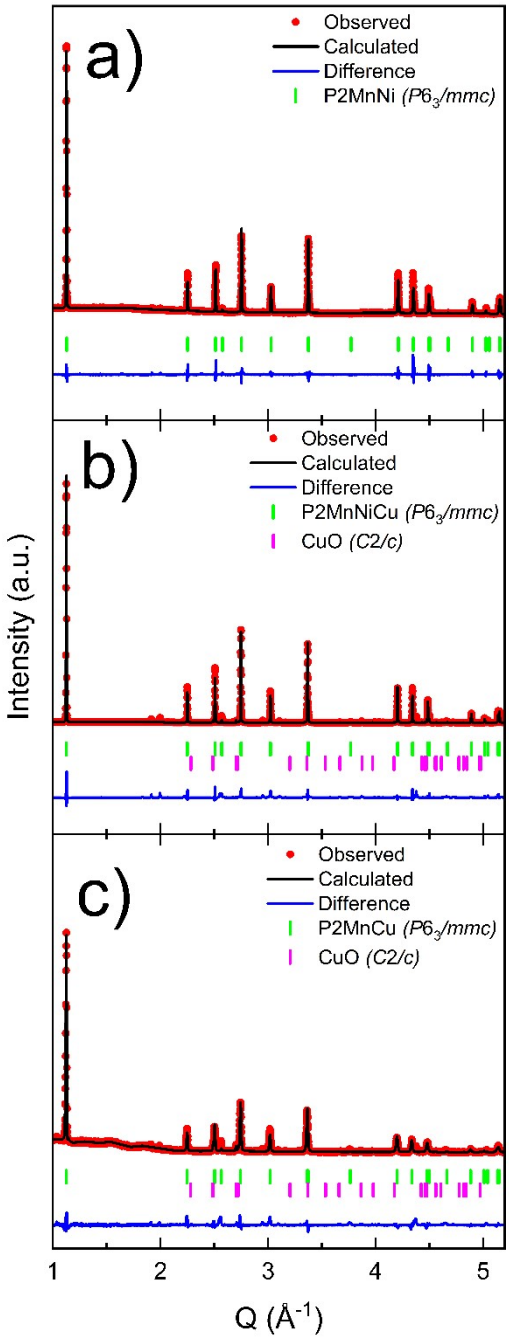

Figure S3. *Rietveld refinements of (a) P2MnNi, (b) P2MnNiCu and (c) P2MnCu materials. Red dots represent the observed XRD data, black lines the calculated diffraction patterns, and blue lines the difference between observed and calculated intensities. Vertical green ticks mark Bragg peak positions of the refined phase, while magenta ticks indicate Bragg peaks of CuO impurity.*

Table S1. *Crystallographic data of P2MnNi calculated from Rietveld refinement of XRD pattern.*

Phase 1: P2 phase (100 wt%)

Space group: *P*6$_3$/*mmc*					
Atom	X	Y	Z	B_{iso} (Å^2)	Occupancy
O1	0.66670	0.33330	0.08702(1)	0.70(9)	2.000
Mn1	0.00000	0.00000	0.00000	0.67(3)	0.667
Ni1	0.00000	0.00000	0.00000	0.67(3)	0.333
Na1	0.00000	0.00000	0.25000	5.3(4)*	0.260(4)
Na2	0.33330	0.66667	0.25000	5.3(4)*	0.407(4)

a = b = 2.88688(1) Å, c = 11.1566(1) Å, α = β = 90 °, γ = 120 °, V = 80.524(1) Å^3

R_p = 20.4, R_{wp} = 21.2, R_{exp} = 5.9, χ^2 = 12.9

Table S2. *Crystallographic data of P2MnNiCu calculated from Rietveld refinement of XRD pattern.*

Phase 1: P2 phase (99.3wt% ± 0.6)

Space group: *P*6$_3$/*mmc*					
Atom	X	Y	Z	B_{iso} (Å^2)	Occupancy
O1	0.66670	0.33330	0.08794(1)	0.667(6)	2.000
Mn1	0.00000	0.00000	0.00000	0.868(2)	0.667
Ni1	0.00000	0.00000	0.00000	0.868(2)	0.167
Cu1	0.00000	0.00000	0.00000	0.868(2)	0.167
Na1	0.00000	0.00000	0.25000	6.8(5)*	0.253(5)
Na2	0.33330	0.66670	0.25000	6.5(5)*	0.414(5)

a = b = 2.89308(1) Å, c = 11.1684(1) Å, α = β = 90 °, γ = 120 °, V = 80.954(1) Å^3

Phase 2: CuO (0.7wt% ± 0.1)

a = 4.6877(5) Å, b = 3.4246(3) Å, c = 5.1327(5) Å, α = γ = 90 °, β = 99.53(7) °, V = 81.258(1) Å^3

R_p = 21.6, R_{wp} = 28.2, R_{exp} = 0.58, χ^2 = 2380

Table S3*. Crystallographic data of P2MnCu calculated from Rietveld refinement of XRD pattern.*

Phase 1: P2 phase (97.9wt% ± 1.1)

Space group: *P*6$_3$/*mmc*					
Atom	X	Y	Z	B_{iso} (Å^2)	Occupancy
O1	0.66670	0.33330	0.08866(1)	0.143(1)	2.000
Mn1	0.00000	0.00000	0.00000	0.986(1)	0.667
Cu1	0.00000	0.00000	0.00000	0.986(1)	0.333
Na1	0.00000	0.00000	0.25000	6.6(9)*	0.270(2)
Na2	0.33330	0.66670	0.25000	8.5(9)*	0.395(2)

a = b = 2.8969(1) Å, c = 11.1756(1) Å, α = β = 90 °, γ = 120 °, V = 81.219(1) Å^3

Phase 2: CuO (2.1wt% ± 0.2)

a = 4.68009(1) Å, b = 3.43357(1) Å, c = 5.12555(1) Å, α = γ = 90 °, β = 99.52774(1) °, V = 81.228(1) Å^3

R_p = 31.1, R_{wp} = 36.5, R_{exp} = 13.95, χ^2 = 6.86

*The large B_{iso} values for sodium reflect its high mobility in the prismatic position.

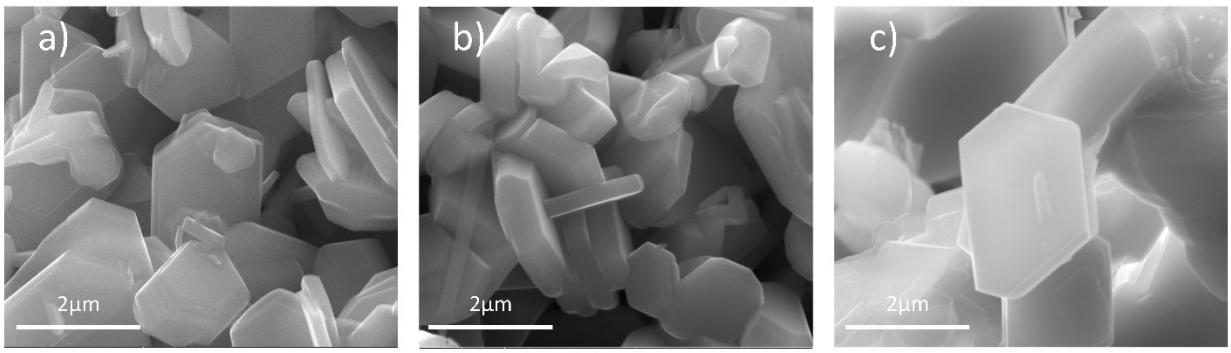

Figure S4*. SEM images of (a) P2MnNi, (b) P2MnNiCu and (c) P2MnCu materials.*

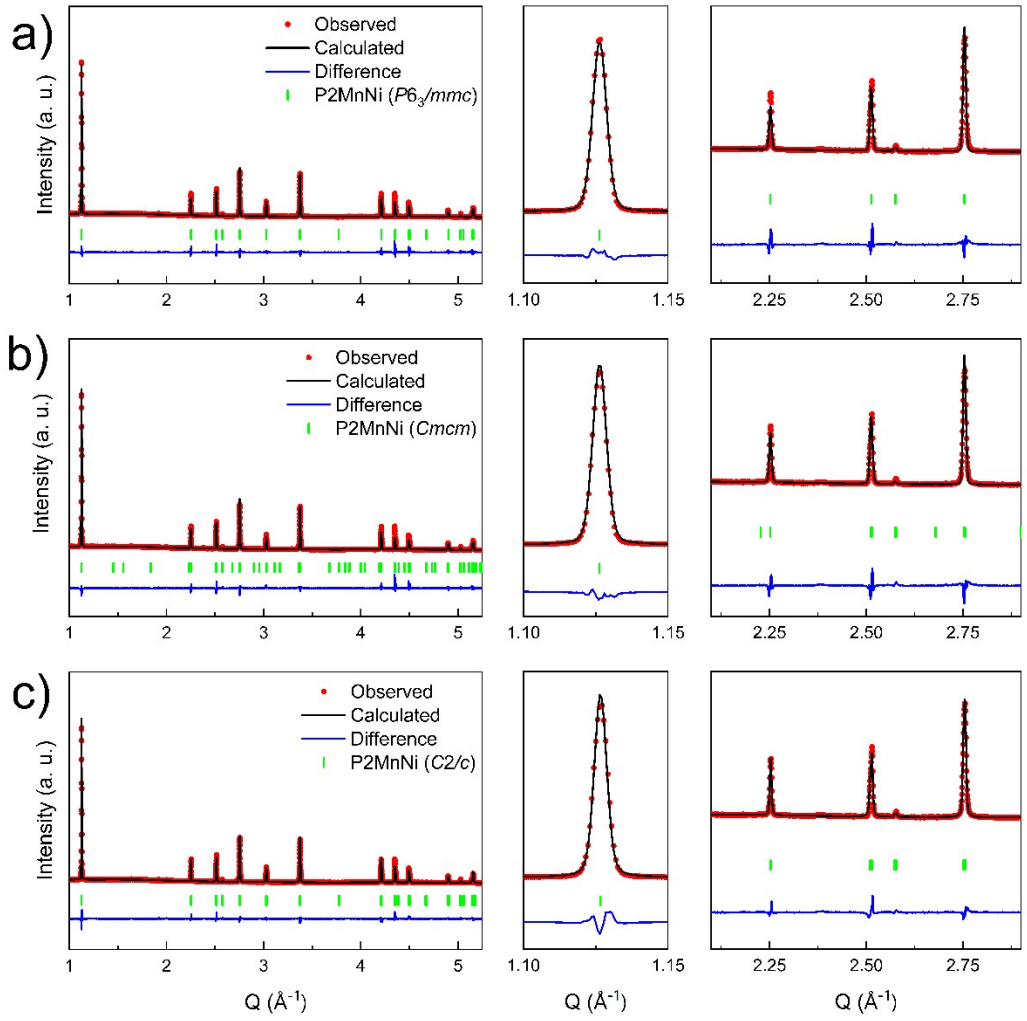

Figure S5. *Rietveld refinements of $Na_{2/3}Mn_{2/3}Ni_{1/3}O_2$ using (a) $P6_3/mmc$ (b) Cmcm and (c) C2/c space groups. The left panels show the full diffraction patterns, while the middle and right panels display enlarged views of selected Q regions (1.10–1.15 $Å^{-1}$ and 2.1–2.9 $Å^{-1}$, respectively). Red dots represent the observed XRD data, black lines the calculated diffraction patterns, and blue lines the difference between observed and calculated intensities. Vertical green ticks mark Bragg peak positions of the refined phase.*

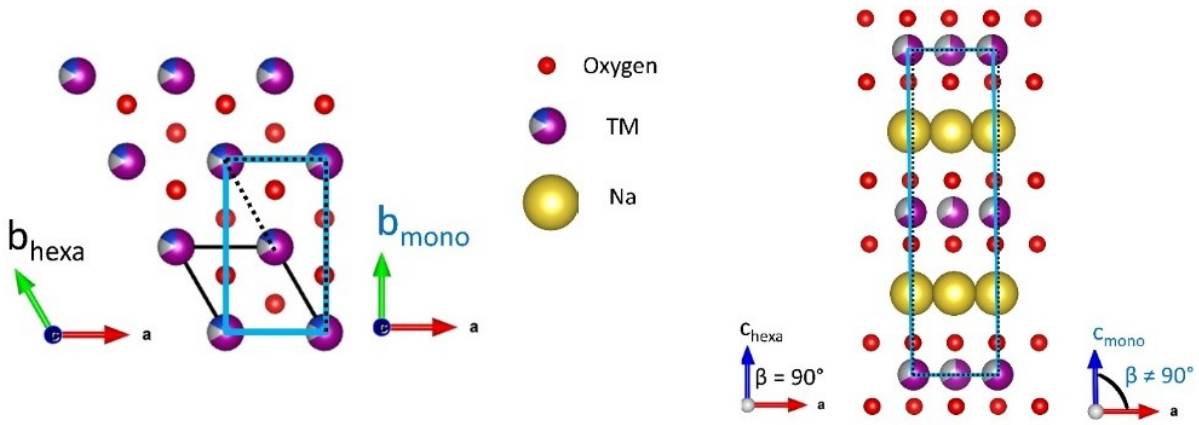

Figure S6. *Comparison of hexagonal and monoclinic unit cell representations (left) in the a–b plane and (right) in the a–c plane. Since different space groups have been used, corresponding to different unit cells, the values for the C2/c space group used for P2MnNi and P2MnCu are transformed into the hexagonal unit cell for comparative purposes by applying the following transformation:* $a_{hexa} = a_{mono}$, $b_{hexa} = \frac{1}{2}\sqrt{b_{mono}^{2} + a_{mono}^{2}}$ *and* $c_{hexa} = c_{mono}/sin(\beta)$.

Table S4*. Crystallographic data of P2MnNi ($Na_{2/3}Mn_{2/3}Ni_{1/3}O_2$) calculated from Rietveld refinement of XRD pattern using Cmcm space group.*

Space group: *Cmcm*					
Atom	X	Y	Z	B_{iso} (Å^2)	Occupancy
O1	0.00000	0.33333	0.59060	0.559(1)	1.000
O2	0.00000	0.16667	0.08794	0.295(1)	1.000
Mn1	0.00000	0.00000	0.00000	0.360(1)	0.666
Ni1	0.00000	0.00000	0.00000	0.586(2)	0.333
Na1	0.00000	0.00000	0.25000	4.3(9)	0.085(2)
Na2	0.00000	0. 33333	0.25000	7.3(9)	0.134(1)
Na3	0.16667	0.50000	0.25000	5.6(9)	0.171(2)
Na4	0.16667	0.16667	0.75000	3.4(9)	0.271(2)

a = 8.667037(2) Å, b = 4.99638(1) Å, c = 11.1566(2) Å, α = β = γ = 90 °, V = 483.124(1) Å^3

R_p = 22.3, R_{wp} = 21.3, R_{exp} = 6.55, χ^2 = 10.6

Table S5. *Crystallographic data of P2MnNi ($Na_{2/3}Mn_{2/3}Ni_{1/3}O_2$) calculated from Rietveld refinement of XRD pattern using C2/c space group.*

Space group: *C2/c*					
Atom	X	Y	Z	B_{iso} (Å^2)	Occupancy
O1	0.00000	0.33333	0.58852	0.306(1)	1.000
Mn1	0.00000	0.00000	0.00000	0.155(1)	0.666
Ni1	0.00000	0.00000	0.00000	0.155(1)	0.333
Na1	0.00000	0.00000	0.25000	2.7(2)	0.374(1)
Na2	0.00000	0. 33333	0.25000	9.2(3)	0.334(1)

a = 2.88292(1) Å, b = 5.00626(1) Å, c = 11.15358(1) Å, α = γ = 90 °,

β = 90.07433(2) °, V = 160.975(1) Å^3

R_p = 14.8, R_{wp} = 15, R_{exp} = 5, χ^2 = 9.03

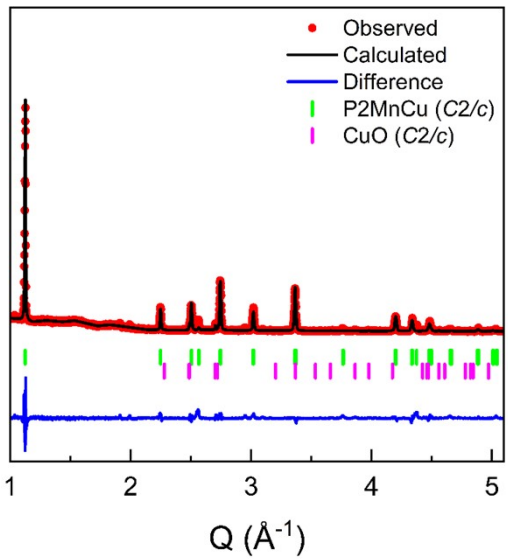

Figure S7. *Rietveld refinement of $Na_{2/3}Mn_{2/3}Cu_{1/3}O_2$ material. Red dots represent the observed XRD data, black lines the calculated diffraction patterns, and blue lines the difference between observed and calculated intensities. Vertical green ticks mark Bragg peak positions of the refined phase, while magenta ticks indicate Bragg peaks of CuO impurity.*

Table S6*. Crystallographic data of P2MnCu ($Na_{2/3}Mn_{2/3}Cu_{1/3}O_2$) calculated from Rietveld refinement of XRD pattern.*

Phase 1: P2 phase (98.1wt% ± 1.3)

Space group: *C2/c*					
Atom	X	Y	Z	B_{iso} (Å^2)	Occupancy
O1	0.00000	0.33333	0.59060	0.318(1)	1.000
Mn1	0.00000	0.00000	0.00000	0.854(2)	0.666
Cu1	0.00000	0.00000	0.00000	0.854(2)	0.333
Na1	0.00000	0.00000	0.25000	9.8(9)	0.362(2)
Na2	0.00000	0. 33333	0.25000	4.7(9)	0.308(2)

a = 2.8989(1) Å, b = 5.01351(1) Å, c = 11.17253(1) Å, α = γ = 90 °,

β = 90.07102(2) °, V = 162.378(1) Å^3

Phase 2: CuO (1.9wt% ± 0.2)

a = 4.68009(1) Å, b = 3.43357(0) Å, c = 5.12555(1) Å, α = γ = 90 °,

β = 99.52774(1) °, V = 81.228(1) Å^3

R_p = 36.1, R_{wp} = 39.6, R_{exp} = 13.94, χ^2 = 8.06

Table S7. *Comparison of electrochemical performances of different materials at C/10, between 2.0 – 4.2V vs Na^+/Na.*

Materials	**Initial discharge capacity (mAh g^{-1})**	**Capacity retention after 50 cycles**	**Capacity retention after 100 cycles**
$Na_{2/3}Mn_{2/3}Ni_{1/3}O_2$	131.6	52%	37%
$Na_{2/3}Mn_{2/3}Cu_{1/6}Ni_{1/6}O_2$	92.9	97%	92%
$Na_{2/3}Mn_{2/3}Cu_{1/3}O_2$	93.4	41%	N/A

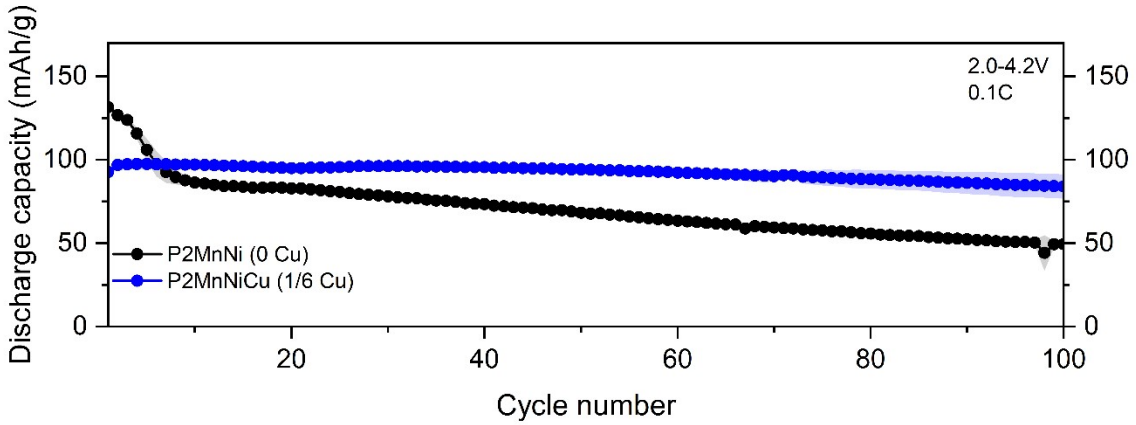

Figure S8. *Capacity retention plot in half cell for P2MnNi and P2MnNiCu in the 2.0–4.2 V voltage window for 100 cycles. The cycling data represent the average values obtained from independent cells, with the shaded area indicating the standard deviation.*

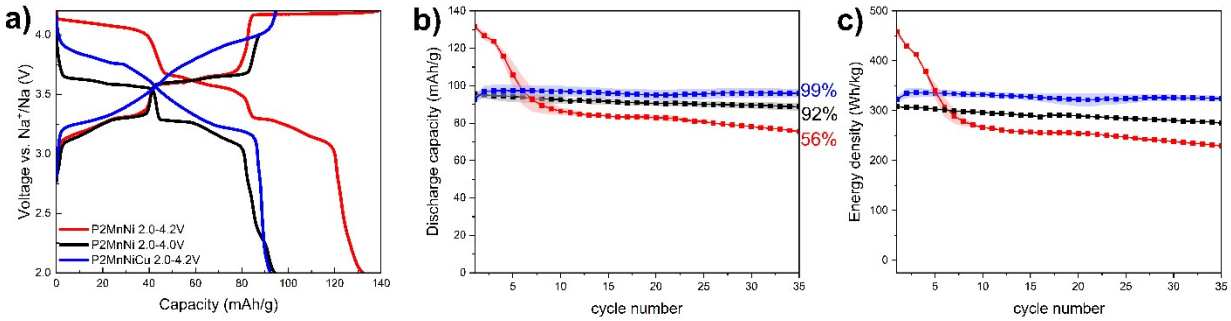

Figure S9. *(a) Electrochemical performance of P2MnNi under different voltage windows compared to P2MnNiCu material. (b) Discharge capacity and (c) energy density vs. cycle number over 35 cycles. The cycling data represent the average values obtained from independent cells, with the shaded area indicating the standard deviation.*

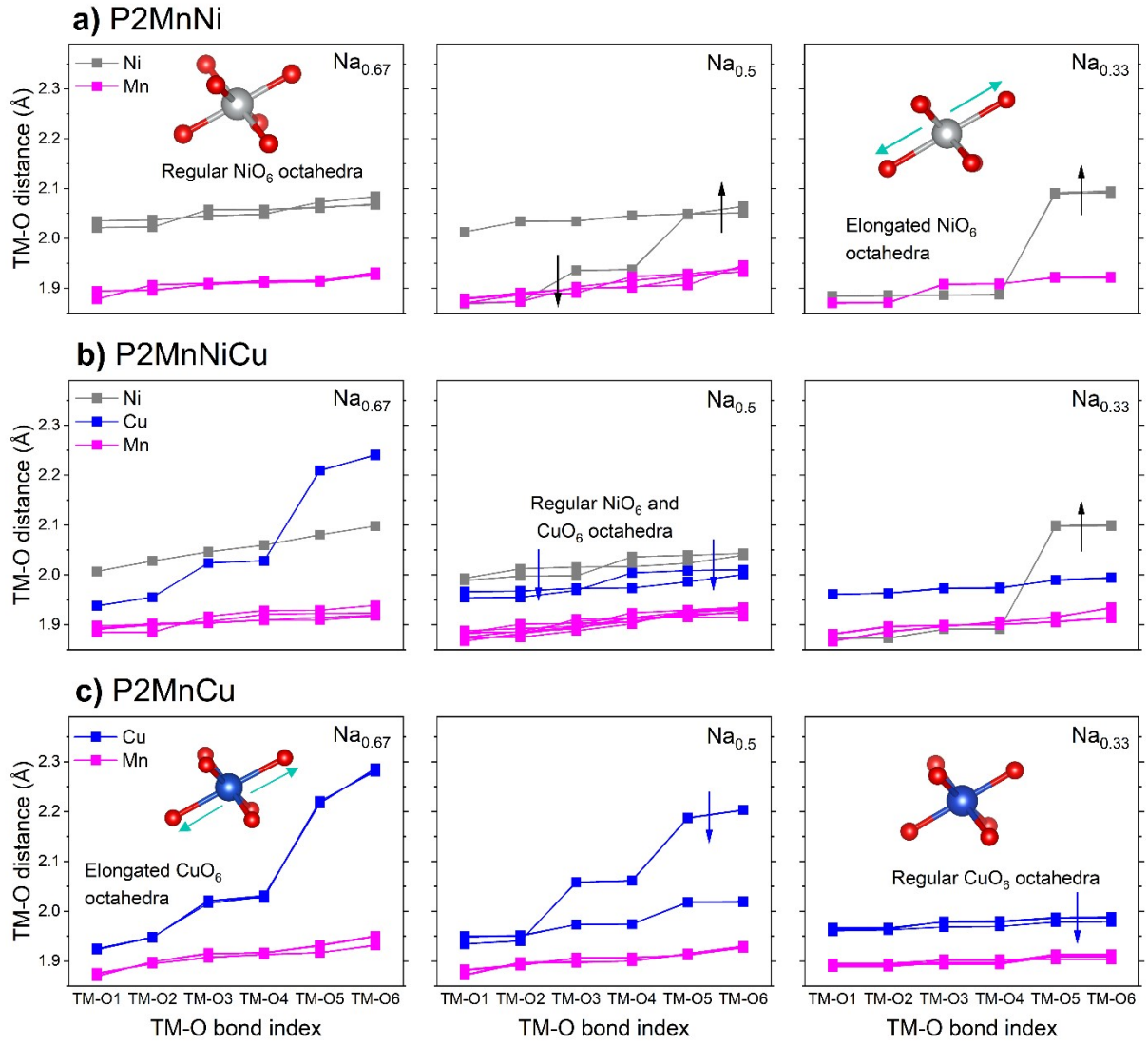

Figure S10. *Evolution of individual TM–O bond distances in (a) P2MnNi, (b) P2MnNiCu, and (c) P2MnCu at Na contents of 0.67, 0.50, and 0.33. TM–O bond indices (1–6) correspond to the six metal–oxygen distances around each transition metal, ordered by increasing length. Data are extracted from fully relaxed DFT structures (see section 2.6.). Colours indicate the transition metal species (Mn, Ni, Cu), and insets illustrate the emergence or suppression of octahedral distortions.*

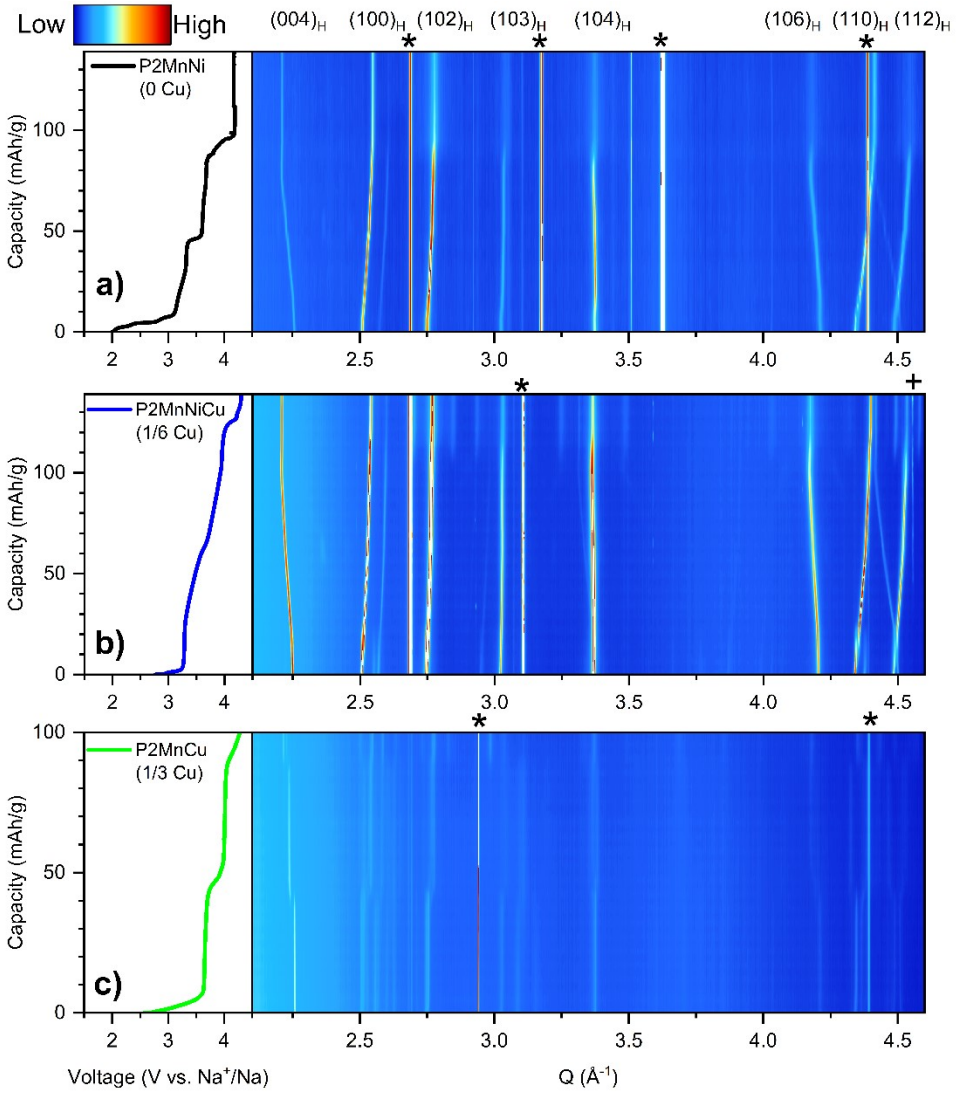

Figure S11. *Complete operando SXRD contour plots during charge for (a) P2MnNi, (b) P2MnNiCu and (c) P2MnCu over the full Q–range. * and + markers indicate peak positions of Al and Na metal arising from the cell stack.*

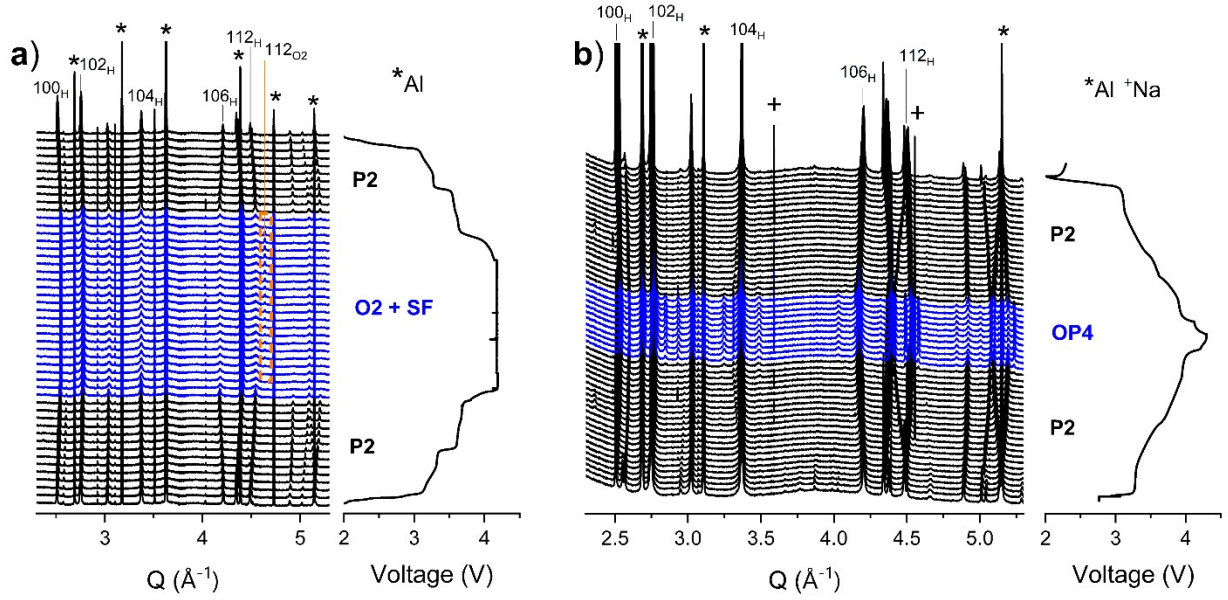

Figure S12. *Operando SXRD during a full cycle for (a) P2MnNi and (b) P2MnNiCu. * and + markers indicate peak positions of Al and Na metal arising from the cell stack.*

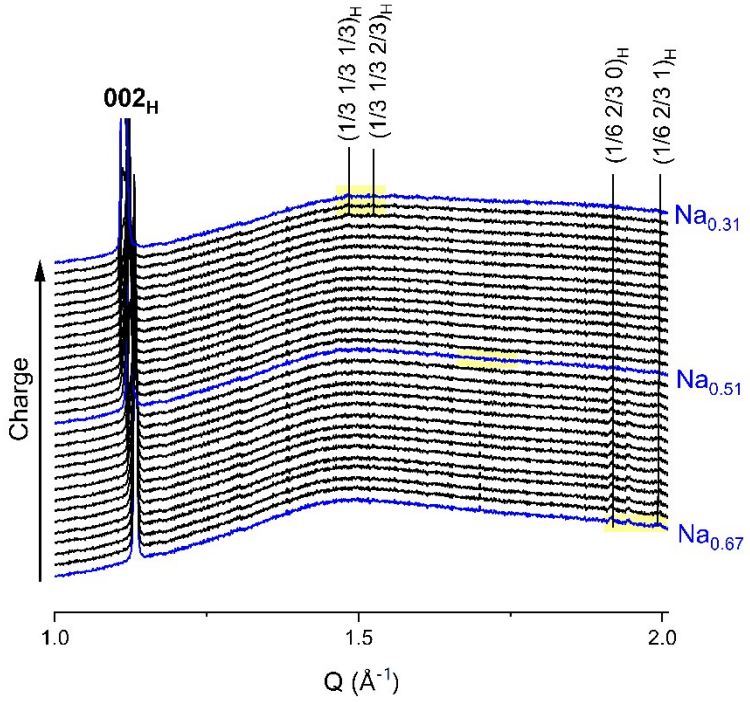

Figure S13. *Operando SXRD during the first charge between Q = 1 – 2 Å^{-1} for P2MnCu.*

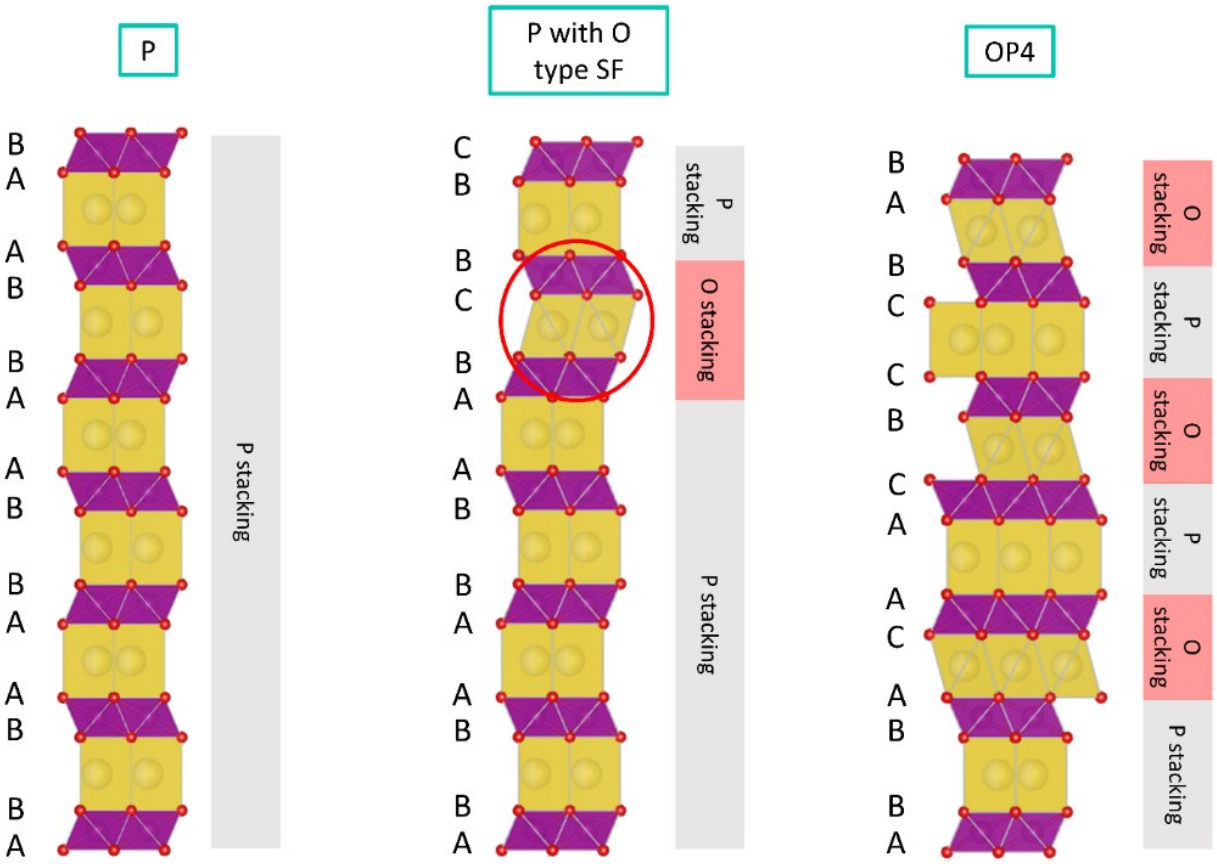

Figure S14. *Comparison of stacking arrangements in layered oxides. From left to right: ideal P2 structure with prismatic Na coordination (ABBA sequence); P2 structure containing a local O–type stacking fault, highlighted in red, where octahedral Na coordination occurs (ABC segment); OP4 structure showing alternating P and O stacking blocks, corresponding to ABBA–CAAC–BCCB repetition.*

Table S8. *Cell parameters and atomic positions used to describe the P2-to-O2 FAULTS model.*

Cell Parameters:					
$a = b = 2.89645$ Å $c = 11.1771$ Å			$\alpha = \beta = 90^o$ $\gamma = 120^o$		
Layer 1 (P-type)					
Atom	x	y	z	Occupancy	B_{iso}
O1	0.33333	0.66667	0.33784	1	0
O2	0.66667	0.33333	0.16216	1	0
Mn1	0	0	0.25	1	0
Na1	0	0	0	0.5	0
Na2	0.33333	0.66667	0	0.5	0
Layer 2 (P-type)					
Atom	x	y	z	Occupancy	B_{iso}
O1	0.66667	0.33333	0.33784	1	0
O2	0.33333	0.66667	0.16216	1	0
Mn1	0	0	0.25	1	0
Na1	0	0	0	0.5	0
Na2	0.66667	0.33333	0	0.5	0
Layer 3 (O-type)					
Atom	x	y	z	Occupancy	B_{iso}
O1	0.33333	0.66667	0.33784	1	0
O2	0.66667	0.33333	0.16216	1	0
Mn1	0	0	0.25	1	0
Na1	0	0	0.025	1	0
Layer 4 (O-type)					
Atom	x	y	z	Occupancy	B_{iso}
O1	0.33333	0.66667	0.33784	1	0
O2	0	0	0.16216	1	0
Mn1	0.66667	0.33333	0.25	1	0
Na1	0.33333	0.66667	0.025	1	0
Layer 5 (O-type)					
Atom	x	y	z	Occupancy	B_{iso}
O1	0.33333	0.66667	0.33784	1	0
O2	0.66667	0.33333	0.16216	1	0
Mn1	0	0	0.25	1	0
Na1	0.33333	0.66667	0.025	1	0
Layer 6 (O-type)					
Atom	x	y	z	Occupancy	B_{iso}
O1	0.33333	0.66667	0.33784	1	0
O2	0	0	0.16216	1	0
Mn1	0.66667	0.33333	0.25	1	0

Na1	0.33333	0.66667	0.025	1	0

Table S9. *Transition vector probabilities and translation vectors used in the FAULTS model to generate a P2 structure with 10% of O–type stacking faults.*

Translation vectors:				
Translation	Probability	x	y	z
L1 → L2	90%	0	0	0.5
L1 → L4	5%	0	0	0.45
L1 → L6	5%	0.66667	0.33333	0.45
L2 → L1	90%	0	0	0.5
L2 → L3	5%	0.33333	0.66667	0.45
L2 → L5	5%	0. 66667	0.33333	0.45
L3 → L2	90%	0	0	0.5
L3 → L4	10%	0	0	0.45
L4 → L1	90%	0.66667	0.33333	0.5
L4 → L3	10%	0	0	0.45
L5 → L2	90%	0	0	0.5
L5 → L6	10%	0.66667	0.33333	0.45
L6 → L1	90%	0.66667	0.33333	0.5
L6 → L5	10%	0.33333	0.66667	0.45

Table S8 and **Table S9** show the used layers and transition vectors to generate a P2 structure with a 10% of O-type stacking faults using FAULTS. Layers 1 and 2 correspond to P–type stacking sequence, while layers 3–6 correspond to O–type stacking sequence. Note that odd layer numbers refer to a specific MO_6 octahedra orientation while even layer numbers refer to the inverted orientation. Therefore, only transitions even–odd–even are permitted in this simulation. The O–type layers require to be duplicated to ensure a proper location of the sodium atom within the interlayers. Also note that the P–O transition distance is shorter than P–P in the *z* direction because the O–O interlayer distance is known to be shorter. Also, the atomic position of Na in the O–type layers do not lay at z = 0 but instead at z = 0.025. The reason for this is to ensure that the Na atom stays in the proper position within the transitions.

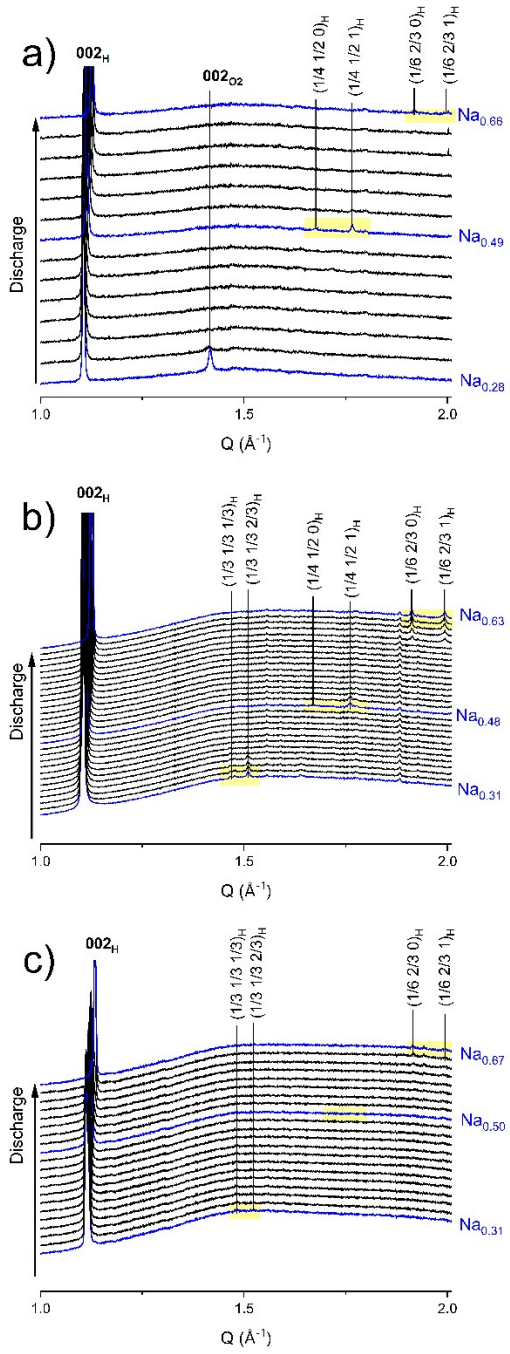

Figure S15. *Operando SXRD during the first discharge between Q = 1 – 2 Å^{-1} for (a) P2MnNi, (b) P2MnNiCu and (c) P2MnCu.*

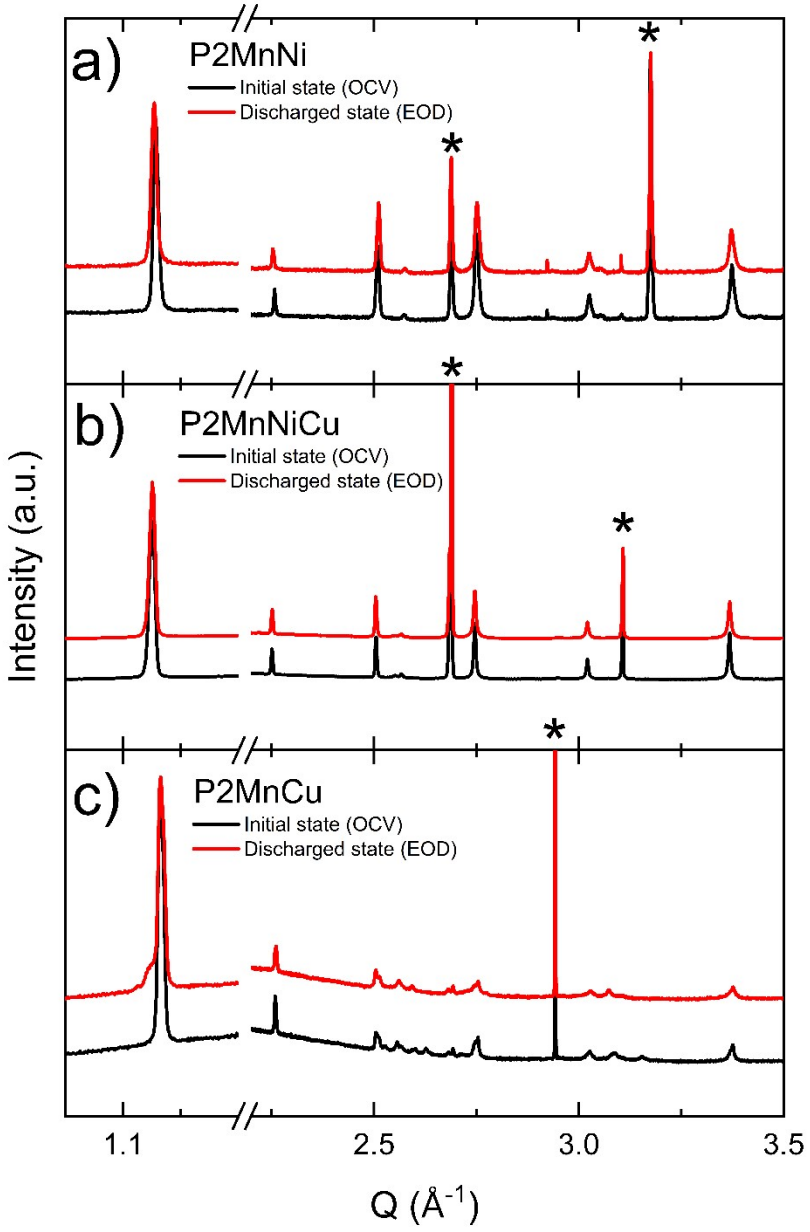

Figure S16. *Operando SXRD of (a) P2MnNi, (b) P2MnNiCu, and (c) P2MnCu at open–circuit voltage (OCV, black) and end of discharge (EOD, red). The * markers indicate peak positions of Al arising from the cell stack.*

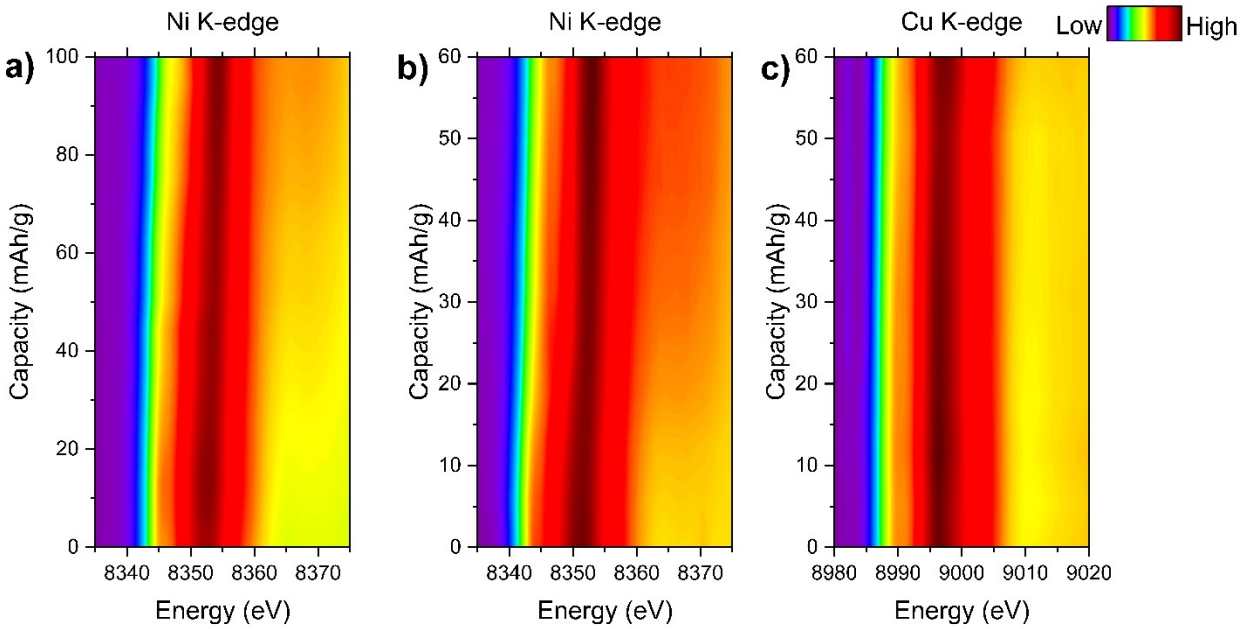

Figure S17. *Contour plots of normalized XANES spectra collected operando during charge as function of capacity. Panel (a) corresponds to the Ni K–edge in P2MnNi, while panels (b) and (c) show the Ni and Cu K–edges, respectively, in P2MnNiCu. The evolution of edge position and spectral features highlights the distinct redox behaviour of Ni and Cu across the charge process.*

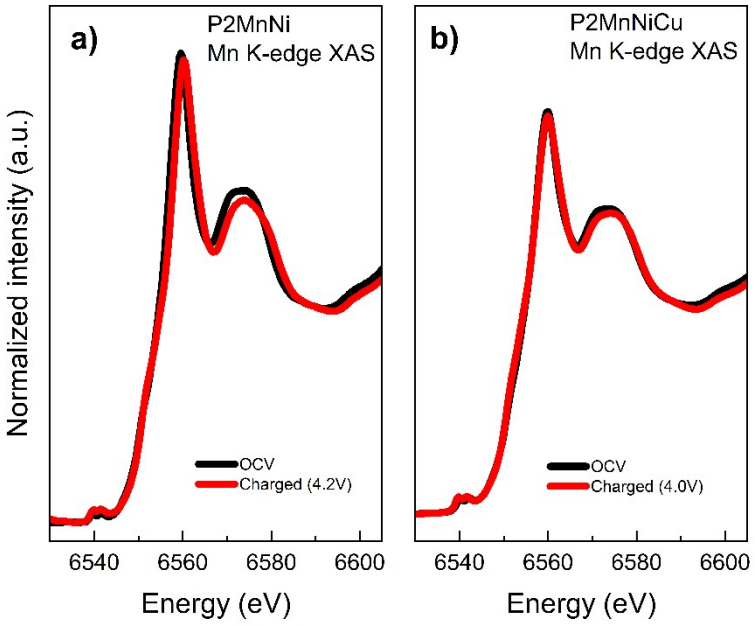

Figure S18. *The Mn K–edge XANES spectra at OCV and charged state in (a) P2MnNi and (b) P2MnNiCu materials.*

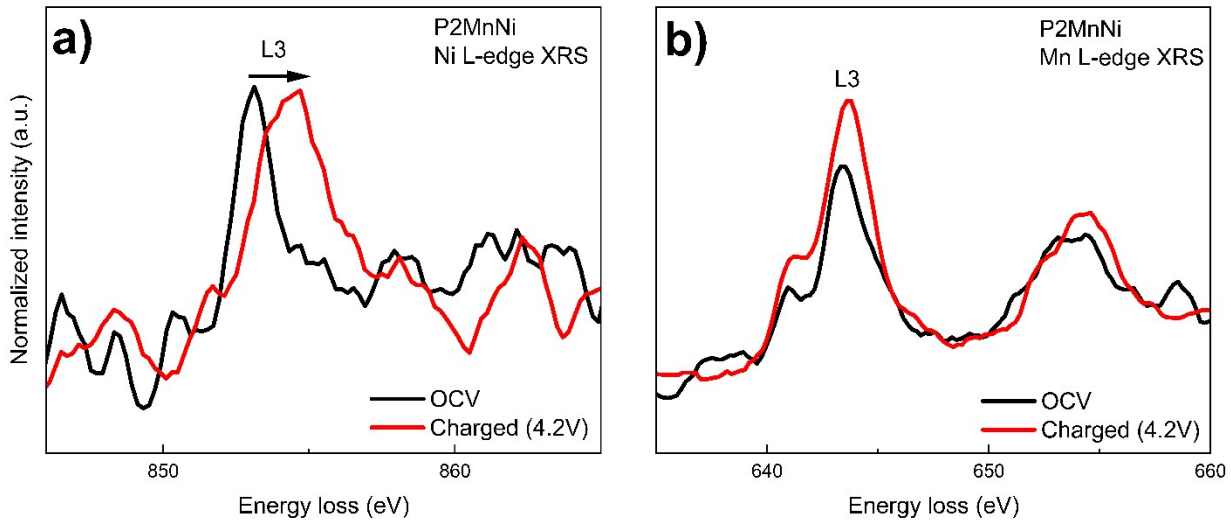

Figure S19. *Ex situ X–ray Raman scattering spectra of (a) Ni L–edge and (b) Mn L–edge at different charge states for P2MnNi material.*

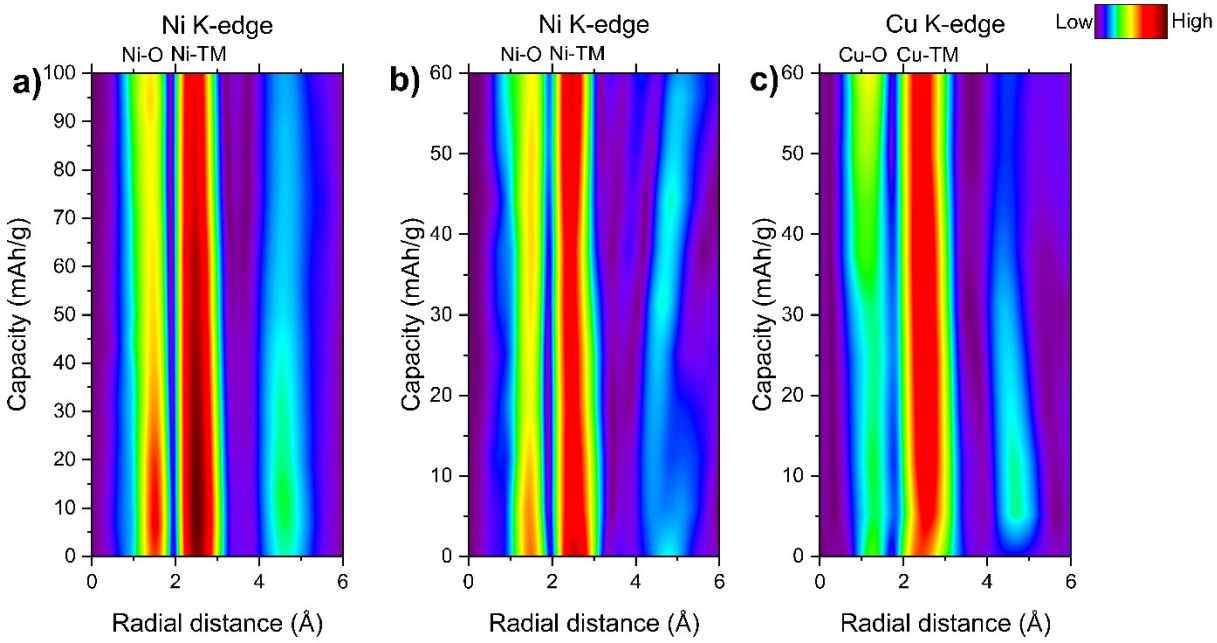

Figure S20. *Contour plots of Fourier Transform Operando EXAFS of P2MnNi and P2MnNiCu during charge. (a) Evolution of the Ni–O and Ni–TM shells in P2MnNi as a function of capacity. (b) Evolution of the Ni–O/Ni–TM and (c) Cu–O/Cu–TM shells in P2MnNiCu. The reciprocal changes in amplitude—decrease of the Ni–O shell intensity and increase of the Cu–O shell intensity—highlight the sequential involvement of Ni and Cu in charge compensation.*

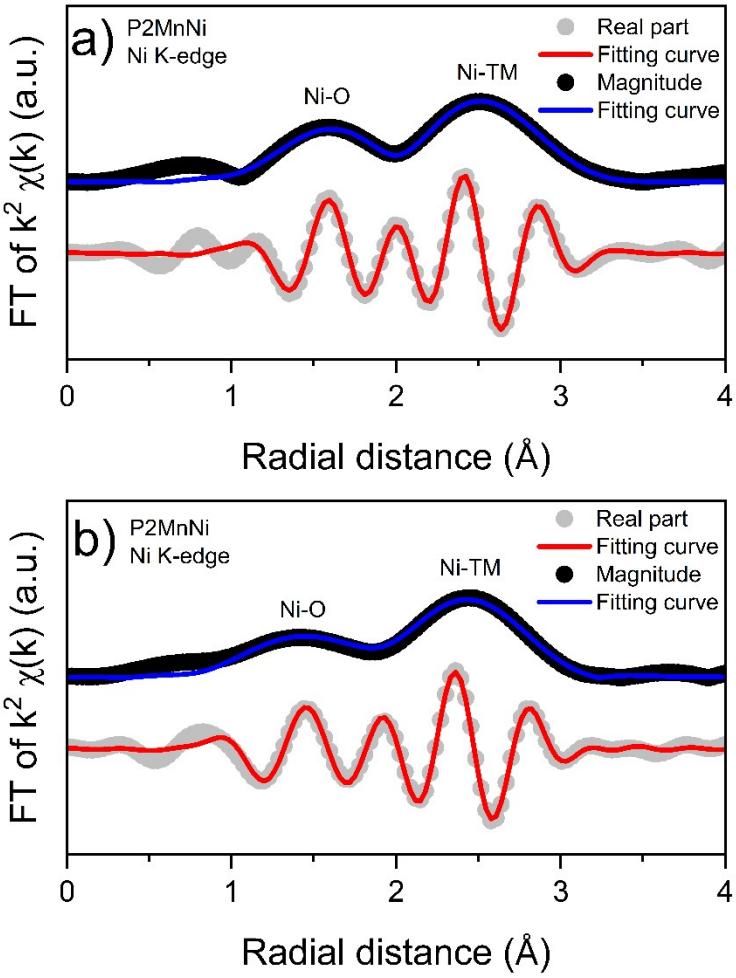

Figure S21. *Representative EXAFS fits in R–space at the Ni K–edge for P2MnNi at (a) open–circuit voltage (OCV) and (b) end of charge (EOC). Fourier–transformed EXAFS spectra and corresponding fits are shown as a function of radial distance.*

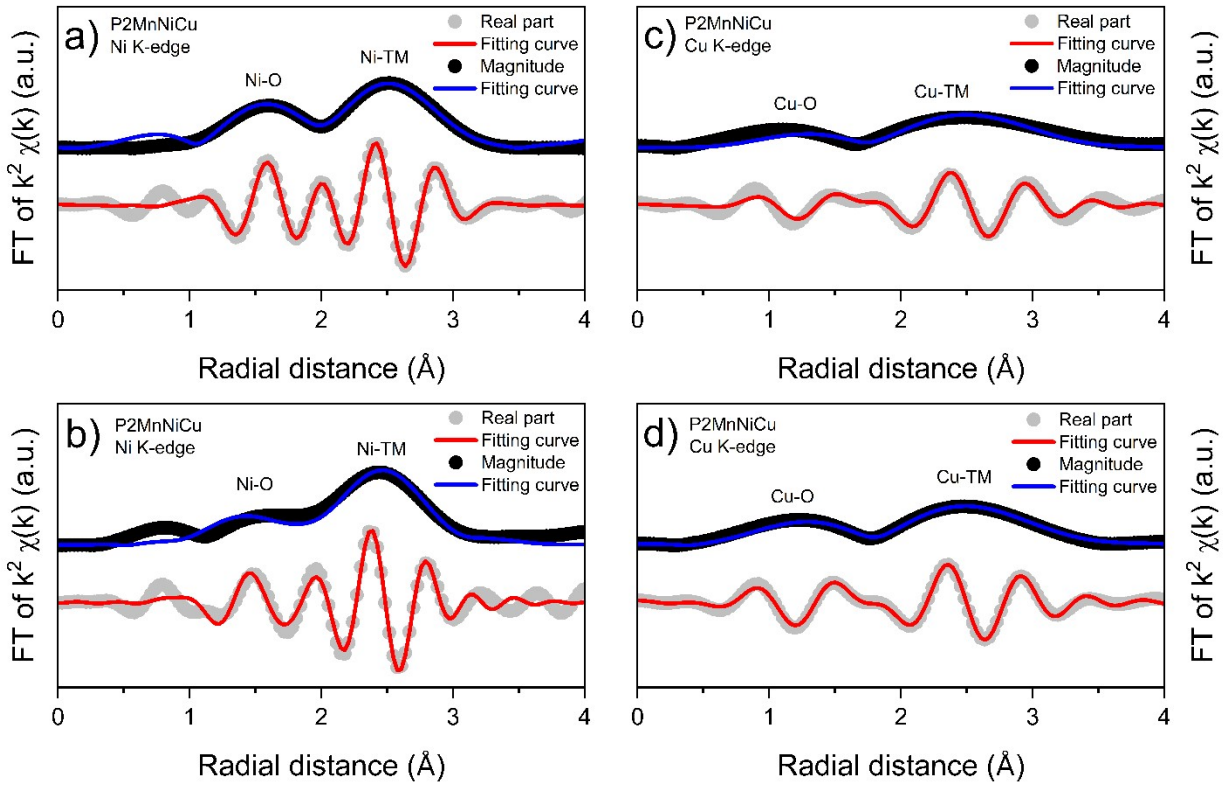

Figure S22. *Representative EXAFS fits in R–space in P2MnNiCu for the Ni K–edge at (a) OCV and (b) charged state and for the Cu K–edge at (c) OCV and (d) charged state. Fourier–transformed EXAFS spectra and corresponding fits are shown as a function of radial distance.*

Table S10. *EXAFS fitting parameters of MCR–ALS components of Ni K–edge in P2MnNi material.*

Component	Shell	*N*	R_{theo} (Å)	R_{fit} (Å)	σ^2 (Å^2)
OCV	TM–O	6	1.986	2.03(6)	0.002(1)
	TM–TM	6	2.885	2.85(2)	0.003(1)
	TM–Na	8	3.248	3.26(1)	0.0004(2)
EOC	TM–O	6	1.986	1.92(6)	0.007(1)
	TM–TM	6	2.885	2.82(6)	0.003(1)
	TM–Na	8	3.248	3.245(3)	0.008(2)

Table S11. *EXAFS fitting parameters of MCR–ALS components of Ni K–edge in P2MnNiCu material.*

Component	Shell	*N*	R_{theo} (Å)	R_{fit} (Å)	σ^2 (Å²)
OCV	TM–O	6	1.986	2.05(8)	0.003(1)
	TM–TM	6	2.885	2.887(2)	0.004(1)
	TM–Na	8	3.248	3.29(4)	0.004(2)
Charged state	TM–O	6	1.986	1.95(1)	0.009(1)
	TM–TM	6	2.885	2.85(2)	0.002(7)
	TM–Na	8	3.248	3.33(8)	0.012(6)

Table S12. *EXAFS fitting parameters of MCR–ALS components of Cu K–edge in P2MnNiCu material.*

Component	Shell	*N*	R_{theo} (Å)	R_{fit} (Å)	σ^2 (Å²)
OCV	TM–O	6	1.986	1.98(1)	0.016(7)
	TM–TM	6	2.885	2.83(8)	0.008(2)
	TM–Na	8	3.248	3.23(5)	0.0004(9)
Charged state	TM–O	6	1.986	1.95(1)	0.007(2)
	TM–TM	6	2.885	2.81(6)	0.003(4)
	TM–Na	8	3.248	3.21(3)	0.001(5)

The amplitude reduction factor was fixed at 0.9 for all fits. EXAFS models including a classical Jahn–Teller–type 4+2 splitting of the TM–O shell were tested but did not improve the fit quality. A simpler single–shell TM–O model was therefore adopted, with the apparent octahedral distortion captured through the Debye–Waller factor.

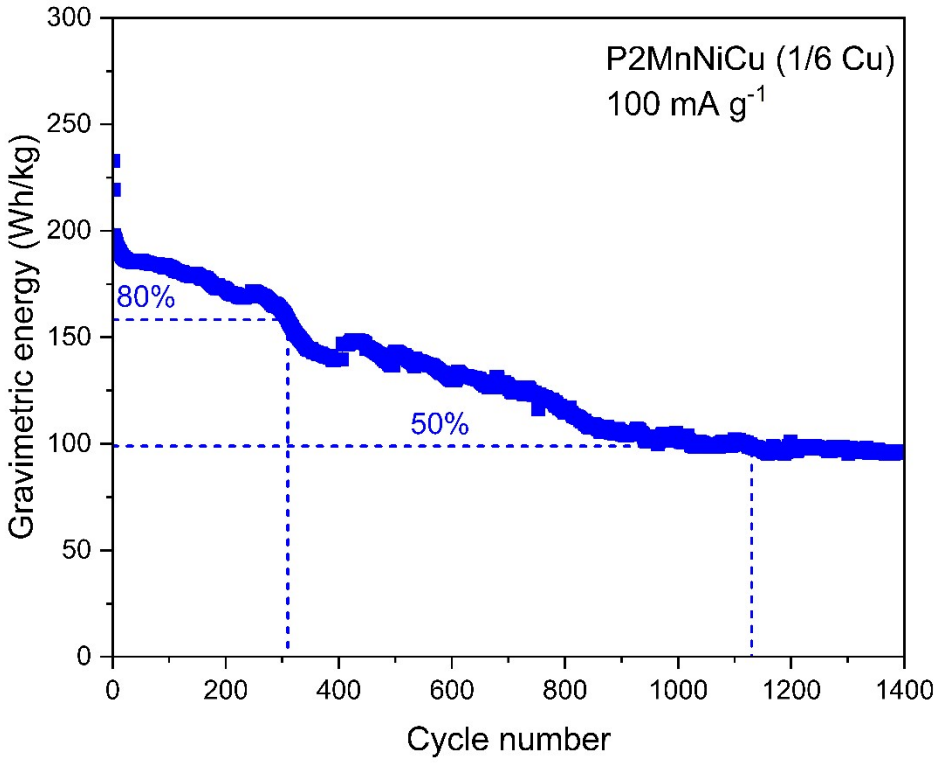

Figure S23. *Extended cycling performance of the full cell of P2MnNiCu material, showing gravimetric energy (Wh kg^{-1}) retention as a function of cycle number. The cell maintains ~80% of its initial gravimetric energy up to 310 cycles and ~50% capacity after 1400 cycles.*

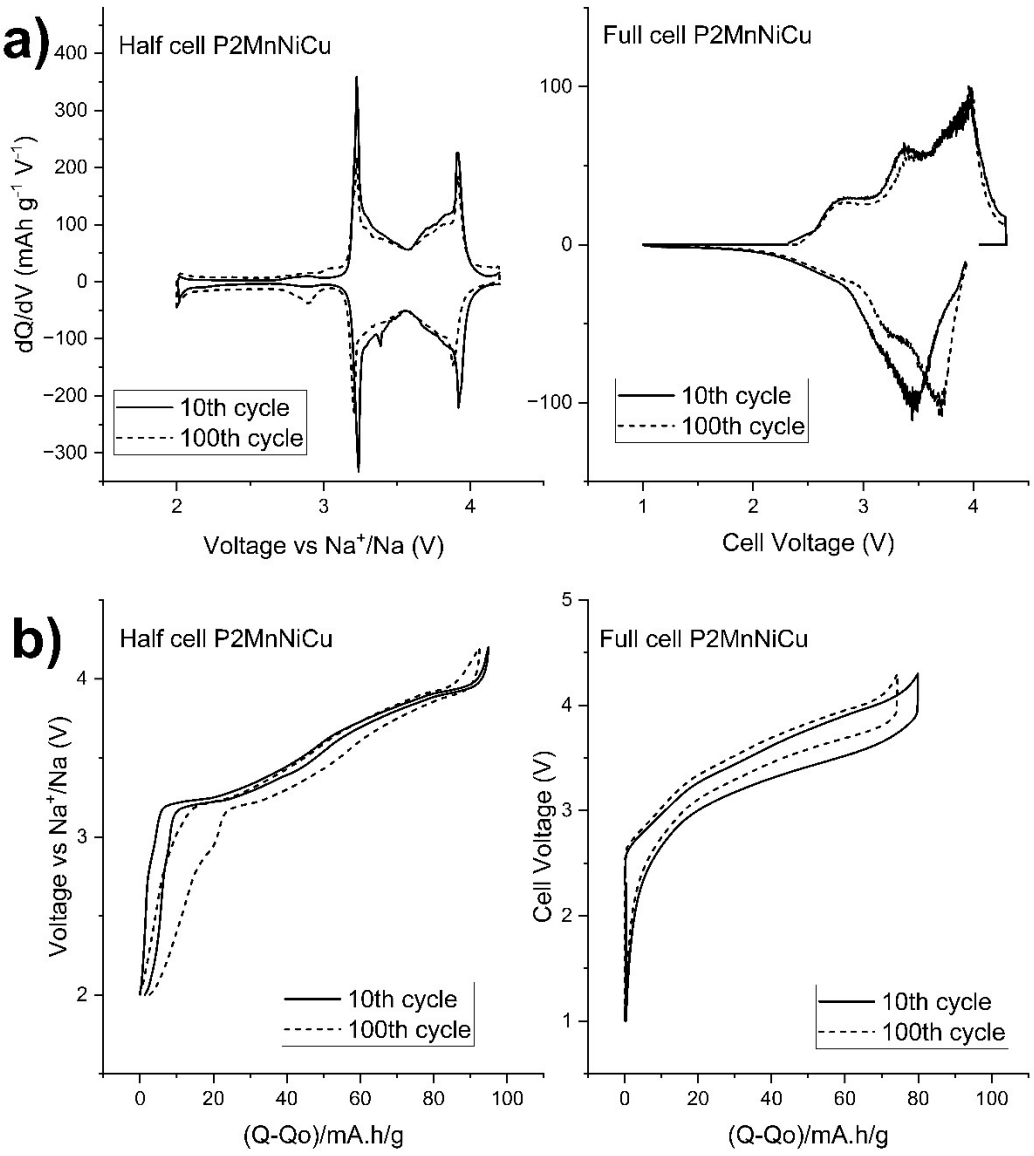

***Figure S24**. Comparison of the electrochemical behaviour of P2MnNiCu in half- and full-cell configurations. (a) Differential capacity (dQ/dV) curves and (b) corresponding voltage profiles of the cycles 10 and 100.*